

VVS: Video-to-Video Retrieval with Irrelevant Frame Suppression

Won Jo¹, Geuntaek Lim¹, Gwangjin Lee¹, Hyunwoo Kim¹, Byungsoo Ko², and Yukyung Choi¹

¹Sejong University

²NAVER Vision

{jwwon, gtlim, gjlee, hwkim}@rcv.sejong.ac.kr

kobiso62@gmail.com ykchoi@rcv.sejong.ac.kr

Abstract

In content-based video retrieval (CBVR), dealing with large-scale collections, efficiency is as important as accuracy. For this reason, several video-level feature-based studies have actively been conducted; nevertheless, owing to the severe difficulty of embedding a lengthy and untrimmed video into a single feature, these studies have shown insufficient for accurate retrieval compared to frame-level feature-based studies. In this paper, we show an insight that appropriate suppression of irrelevant frames can be a clue to overcome the current obstacles of the video-level feature-based approaches. Furthermore, we propose a Video-to-Video Suppression network (VVS) as a solution. The VVS is an end-to-end framework that consists of an easy distractor elimination stage for identifying which frames to remove and a suppression weight generation stage for determining how much to suppress the remaining frames. This structure is intended to effectively describe an untrimmed video with varying content and meaningless information. Its efficacy is proved via extensive experiments, and we show that our approach is not only state-of-the-art in video-level feature-based approaches but also has a fast inference time despite possessing retrieval capabilities close to those of frame-level feature-based approaches.

1. Introduction

Information retrieval is defined as finding the most relevant information in a large collection. It has evolved from finding text within a document [8, 36, 5, 28] to finding images within an image set [2, 38, 15, 19, 18, 9]. In recent years, with the fast-growing trend of the video streaming market, several studies [23, 21, 34, 14, 30] have actively been conducted in content-based video retrieval (CBVR) for finding desired videos from a video set.

The core of CBVR technology is measuring similarities between videos of different lengths, including untrimmed videos. This technique is divided into two streams according to the basic unit for measuring the similarity between two videos: a frame-level feature-based approach and a

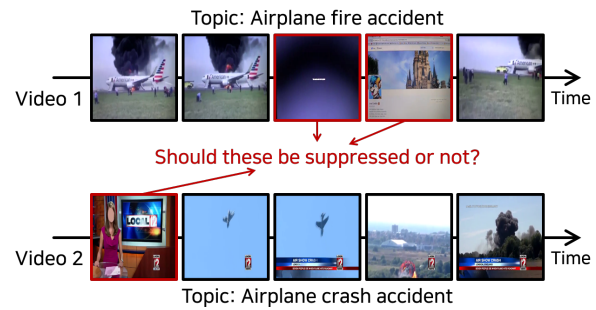


Figure 1: **Q: Should the red boxes be suppressed?** The red boxes in both videos should be excluded because they are not related to the topic in the video, although they are included for a specific purpose or reason. In this work, we demonstrate that the suppression of these red boxes enhances the distinctiveness of features when describing the entire video at once.

video-level feature-based approach. The former aggregates similarities between frame-level features in two videos to calculate a video-to-video similarity. The latter, on the other hand, describes each video as a single feature and computes a video-to-video similarity based on it. These two streams are in a trade-off relationship because the key foundation for determining similarity differs. The frame-level feature-based approach compares each frame directly, it is less dependent on factors such as video duration and whether or not it is trimmed. As a result, relatively accurate searches are possible, but processing speed and memory are expensive due to the necessity of numerous similarity computations and a considerable amount of feature storage space. In comparison, the video-level feature-based approach requires only one similarity calculation between a single pair of features, which is more efficient in terms of processing speed and memory. However, it is difficult to compress many frames of a video into a single feature, so approaches of this type generally exhibit inaccurate search capabilities and also rely on the factors such as duration and trimness.

Ideally, if a video-level feature-based approach could be as distinct as a frame-level approach, it may be the best option in real-world scenarios. However, there are some problems that must be considered. One of them is that distractors in a video interfere with describing video-level features.

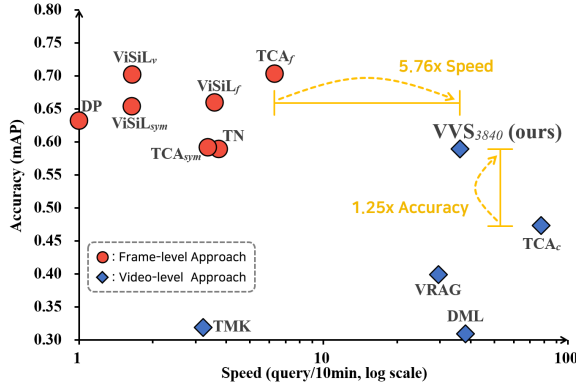


Figure 2: **Speed-Accuracy Comparison on FIVR-200K.** This is a comparison between the proposed approach and existing state-of-the-art approaches in terms of speed and accuracy on the FIVR-200K. The speed is represented by the average number of queries processed in 10 minutes, and the accuracy is represented by the mAP in ISVR, the most difficult task. Further numerical comparisons are provided in the supplementary material.

Distractors in this context refer to frames with visual content unrelated to the main topic. In a video depicting the topic of “Airplane fire accident”, as shown in Figure 1, for instance, the content in the red boxes corresponding to the distractor is unrelated to the topic. A second video of the same figure depicting the topic of “Airplane crash accident” also contains a red box, which does not assist in identifying the topic. In addition to these qualitative instances, we present in the supplementary material an experiment that demonstrates quantitative performance improvements when the distractors are manually eliminated from the previous video-level feature-based schemes. Based on these observations, it is proven that the description of video-level features with optimal suppression of distractors can be an ideal scenario for accurate and fast retrieval.

The objective of this work is to understand the significance of frames in order to determine how much they should be suppressed to produce a distinct video-level feature. To this end, we propose a Video-to-Video Suppression network (VVS). The VVS is an end-to-end framework consisting of two stages: an easy distractor elimination stage for removing frames that can be clearly recognized as distractors, and a suppression weight generation stage for determining how much to suppress the remaining frames via temporal saliency information and relevance of the topic. Our solution is the first explicitly designed framework that employs various signals for relevance, as opposed to earlier approaches [23, 34, 30] where the model was implicitly intended to generate weights. As shown in Figure 2, it achieves the state-of-the-art among video-level feature-based approaches, with search accuracy comparable to frame-level state-of-the-art performance while retaining competitive inference speed. In addition, exten-

sive experiments included in the later section demonstrate the effectiveness of the proposed framework and the validity of the designed structure.

In summary, our main contribution is as follows: 1) We demonstrate an insight that video-level features can be both accurate and fast with proper suppression of irrelevant frames. 2) We propose the VVS, an end-to-end framework for embedding an untrimmed video as a video-level feature while suppressing frames via various signals. 3) Extensive experiments demonstrate the effectiveness of our design, which acquires state-of-the-art performance.

2. Related Work

2.1. Frame-level Feature-based Approaches

Dynamic Programming (DP) [6] detects a near-duplicate region by extracting the diagonal pattern from a frame-level similarity map. Temporal Network (TN) [37] distinguishes the longest route in a graph created by keypoint frame matching to discover visually similar frames between two videos. Circulant Temporal Encoding (CTE) [7] compares frame-level features by using a Fourier transform. This allows frame information to be encoded into the frequency domain. Video Similarity Learning (ViSiL) [21] approach leverages metric learning by basing its operations on a frame-by-frame similarity map. Compact Descriptors for Video Analysis (CDVA) [1] and its variations [29, 25, 27, 14] propose two types of transformation-resistant keyframe features, exploiting complementary abilities between them.

These approaches generally provide more precise search results for a given query than video-level feature-based approaches, although at the expense of considerable time.

2.2. Video-level Feature-based Approaches

Hashing Code (HC) [35] collects and hashes a large number of local and global features to handle accuracy and scalability issues. Deep Metric Learning (DML) [23] utilizes frame-level features from a layer codebook generated for intermediate Maximum Activation of Convolution (iMAC) [22] features and fuses them to represent a video-level feature. Temporal Matching Kernel (TMK) [32] generates a fixed-length sequence for each video, regardless of the total number of frames in the video, using periodic kernels that take frame descriptors and timestamps into consideration. Learning to Align and Match Videos (LAMV) [3] designs a learnable feature transform coefficient based on TMK. Temporal Context Aggregation (TCA) [34] learns frame-level features into video-level features through self-attention and a queue-based training mechanism. Distill-and-Select (DNS) [24] distills the knowledge of the teacher network, which is optimized from the labeled data, into a fine- or coarse-grained student network to take further ad-

vantage of learning from the unlabeled data, and maintains efficiency between the two types of students via a selector network. Video Region Attention Graph (VRAG) [30] learns an embedding for a video by capturing the relationship of region units in frames via graph attention [39] layers.

In general, these approaches can respond to a given query more quickly than frame-level feature-based approaches, even if the response is relatively inaccurate. However, our solution in this category can respond as precisely as frame-level feature-based approaches while being sufficiently fast. In addition, whereas DML, TCA, and VRAG, which are the closest approaches to us, ask FC layers, self-attention layers, and graph attention layers, respectively, to implicitly fuse frame-level features into a video-level feature (that is, only contrastive loss of fused features is used as the objective function), our approach is the first to generate video-level features via explicit signals, such as low-level characteristics, temporal saliency, and topics.

3. Approach

3.1. Preliminaries

Tensor Dot & Chamfer Similarity

Tensor Dot (TD) [41] between two given tensors $\mathcal{A}, \mathcal{B} \in \mathbb{R}^{T \times S^2 \times C}$ is defined as a summation for a specific axis. T , S , and C refer to the temporal, spatial, and channel axes. We only handle the operation on the channel axis; therefore, the output has the size $\mathbb{R}^{T \times S^2 \times S^2 \times T}$. Chamfer Similarity (CS) [4] is defined as the average of the maximum values in the column axis for a given matrix $\mathcal{D} \in \mathbb{R}^{N \times M}$, as shown in Equation (1). If the size of \mathcal{D} is $\mathbb{R}^{T \times S^2 \times S^2 \times T}$, the output size will be $\mathbb{R}^{T \times T}$, and if it is $\mathbb{R}^{T \times T}$, the output size will be \mathbb{R}^1 . Note that these two operations are the same as those introduced in [21].

$$CS(\mathcal{D}) = \frac{1}{N} \sum_{i=1}^N \max_{j \in [1, M]} \mathcal{D}^{(i, j)} \quad (1)$$

Spatio-Temporal Global Average Pooling

Spatio-Temporal Global Average Pooling (ST-GAP) [26] is the global average pooling of the spatial and temporal axes of a given tensor $\mathcal{A} \in \mathbb{R}^{T \times S^2 \times C}$, yielding the output size \mathbb{R}^C . Similarly, Spatial Global Average Pooling (S-GAP) refers to that pooling on the spatial axis alone, with an output of size $\mathbb{R}^{T \times C}$ for the same input. After these two operations, L2 normalization is applied to adjust the difference in scale between tensors.

Diagonal Sampling

Diagonal Sampling (DS) [16] means extracting the diagonal components of a given square matrix $\mathcal{E} \in \mathbb{R}^{T \times T \times C}$. The input we handle with this operation always consists of three axes, and an output of size $\mathbb{R}^{T \times C}$ is generated by sampling from the other two axes besides the channel axis.

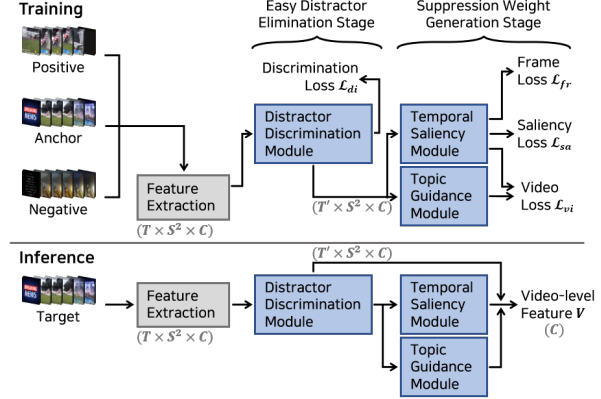


Figure 3: **Pipeline of VVS.** The gray italic letters represent the size of the feature in each process.

3.2. Problem Formulation

Given a video with a length of T , our goal is to embed the video as a video-level feature V while suppressing frames corresponding to distractors. To figure out which frame should be suppressed by how much, the frames of the video are first embedded in the frame-level features $X = \{x^{(t)}\}_{t=1}^T$ instead of being embedded directly in the video-level feature V . Following that, T' frames are chosen by removing easy distractors that are readily identifiable as distractors due to a lack of information via the easy distractor elimination stage. In the subsequent suppression weight generation stage, weights $W = \{w^{(t)}\}_{t=1}^{T'}$ indicating the necessary degree of the remaining frames are then calculated. Consequently, these weights are employed to aggregate frame-level features into a video-level feature $V = \Psi(\{w^{(t)} \otimes x^{(t)}\}_{t=1}^{T'})$, where Ψ represents the ST-GAP and \otimes represents the Hadamard product. This procedure is illustrated in Figure 3.

3.3. Feature Extraction

For the aforementioned reasons, L_N -iMAC as a frame-level feature is first extracted to appropriately compare with many other works [23, 21, 34, 30]. Specifically, each frame is fed to the backbone network Φ as an input, and Regional Maximum Activation of Convolution (R-MAC) [38] is applied to its intermediate feature maps $\mathcal{M}^{(k)} \in \mathbb{R}^{S^2 \times C^{(k)} (k=1, \dots, K)}$. Specifically, after obtaining feature maps from a total of K layers in Φ , N types of region kernels are used depending on the granularity level for applying R-MAC. As a result, each of the K intermediate feature map $\mathcal{M}^{(k)}$ have their own channel $C^{(k)}$ but the same spatial resolution S^2 . After these $\mathcal{M}^{(k)}$ are concatenated on the channel axis, they are generated as a frame-level feature $x \in \mathbb{R}^{S^2 \times C (C=\sum_{k=1}^K C^{(k)})}$. After applying PCA whitening [12] to each of the features x , the L_N -iMAC feature $X \in \mathbb{R}^{T \times S^2 \times C}$ is obtained. Although the dimension of the channel axis could be reduced to dif-

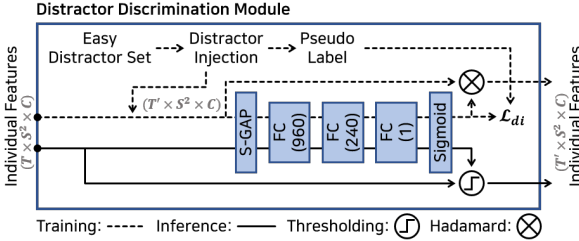


Figure 4: **Pipeline of DDM.** The gray italic letters indicate the size of the feature in each process. The number in parentheses in layer blocks indicates the output dimension.

ferent sizes for comparison with other approaches when applying PCA whitening, for convenience, the dimension of the frame-level feature is referred to as C .

3.4. Easy Distractor Elimination Stage

In this section, we introduce Distractor Discrimination Module (DDM), which eliminates frames that are clearly recognizable as distractors owing to a lack of visual information. An easy distractor is a frame with little variation in pixel intensity and few low-level characteristics (edge, corner, etc.) in an image, such as the third frame of the first video in Figure 1. In the training phase of the DDM, frame-level features corresponding to the easy distractor are injected into an input with a length of T , and the model is optimized to distinguish them. In the inference phase of the DDM, frames predicted as easy distractors are removed from the input. This process results in the output length being longer than the input length T in the training phase but shorter in the inference phase. For convenience, the output length of the DDM is always referred to as T' . The overall DDM flow is depicted in Figure 4.

Distractor Discrimination Module

To enable this module to learn to recognize the easy distractor, we create a pseudo-label using the magnitude of the frame-level features. This is because frames with few low-level characteristics have fewer elements to be activated from the backbone network of L_N -iMAC, which consists of several activation layers, resulting in a smaller magnitude of their intermediate feature map.

Specifically, before the training phase, a set of easy distractors with a magnitude less than or equal to a magnitude threshold λ_{mag} is constructed from all frame-level features of videos in the training dataset. Examples of easy distractors included in this set can be viewed in the supplementary material. During the training phase, features of easy distractors are picked from the set and randomly placed between the features X . In this case, only about 20–50% of T is injected, resulting in features with a length of T' . At the same time, the points where the distractors are injected are set to 0 and the opposite position to 1, resulting in a pseudo-label $Y_{di} = \{y_{di}^{(t)}\}_{t=1}^{T'}$. The injected features

are projected through multiple layers to calculate the confidence $W_{di} = \{w_{di}^{(t)}\}_{t=1}^{T'}$. Due to the fact that only the components within each frame determine the criterion for identifying easy distractors, the multiple layers consist only of FC layers to handle each frame independently without interaction between frames. As a result, this module is optimized through the discrimination loss \mathcal{L}_{di} , computed as the binary cross entropy loss between the confidence W_{di} and the pseudo-label Y_{di} .

The objective of DDM is to convey features to the subsequent stage, erasing features of frames that are deemed to be easy distractors through thresholding for confidence. In this case, as the threshold operation is not differentiable during the training phase, the output is derived from the Hadamard product of the confidence W_{di} and the input features X , and during the inference phase, from a thresholding operation based on a distractor threshold λ_{di} .

3.5. Suppression Weight Generation Stage

Even if the easy distractors are excluded through the previous stage, untrimmed videos still contain hard distractors that cannot be easily distinguished and are unrelated to the overall topic of the video due to the various content entanglements. In this section, Temporal Saliency Module (TSM) and Topic Guidance Module (TGM) are introduced for calculating suppression weights, which indicate how close the remaining frames are to the hard distractor. TSM assesses the significance of each frame based on saliency information derived from frame-level similarities, whereas TGM measures the degree to which each frame relates to the overall topic of the video. The weights obtained from these two modules are converted into the suppression weights W using the Hadamard product.

Temporal Saliency Module

To measure the importance of each frame, saliency information is mined in the training phase. This is inspired by [21], which proposes a model that refines a frame-level similarity map during training and accumulates it to a frame-level similarity via the CS operation. We find that as the model is optimized, the CS operation that prioritizes maximization increases the values of the locations involved in enhancing a video-level similarity between a positive pair in a frame-level similarity map of that pair. The locations with increasing values on the similarity map eventually represent frames that are important for improving the similarity between videos representing related topics; hence, saliency information may be considered to be contained in them. For this reason, this module intends to guide a model by generating saliency information-containing frames into a pseudo-label so that the importance of each frame can be estimated. In addition, an experiment examining whether saliency information derived from frame-level similarities helps to de-

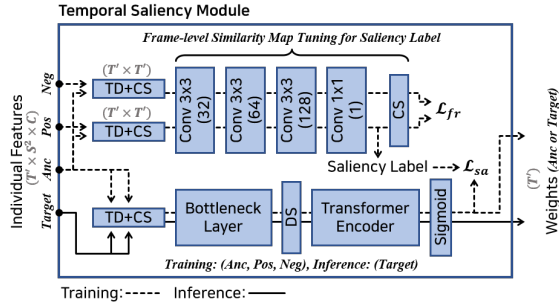


Figure 5: **Pipeline of TSM.** The gray italic letters represent the size of the feature in each process. The number in parentheses in layer blocks indicates the output dimension.

scribe a video-level feature is presented in the supplemental material.

Before explaining the details of the mining, the procedure for obtaining the frame-level similarities of [21] is briefly introduced. First, three sets of frame-level features (in our case, each size is $\mathbb{R}^{T' \times S^2 \times C}$) are described based on a triplet containing an anchor, a positive, and a negative. Then, TD is applied between the features of the anchor and those of the positive to get an output of size $\mathbb{R}^{T' \times S^2 \times S^2 \times T'}$, followed by CS to generate a frame-level similarity map of size $\mathbb{R}^{T' \times T'}$. This process is equally applied between the anchor and the negative to obtain a similarity map of the same size. Here, the rows of the two maps correspond to the indices of the frames within the anchor. The two similarity maps are fed into multiple layers to yield finely tuned similarity maps $\mathcal{D}_p, \mathcal{D}_n \in \mathbb{R}^{T'' \times T''}$, where \mathcal{D}_p stands for a tuned map from the positive pair, \mathcal{D}_n from negative pairs, and T'' the size reduced through the layers. The layer is then optimized with the sum (which we refer to as the frame loss \mathcal{L}_{fr}) of the triplet margin loss between positive and negative scores created by CS operations on these tuned maps and the regularization loss (the input is $\mathcal{D}_p, \mathcal{D}_n$, and the rest is the same as in [21]) that penalizes to prevent these tuned maps from diverging.

As previously mentioned, during the tuning of the frame-level similarity maps, locations holding saliency information become more prominent in the positive pair similarity map \mathcal{D}_p , and a pseudo-label, i.e., a saliency label Y_{sa} , is produced based on these locations:

$$\begin{aligned} \rho_i &= \max_{j \in [1, T'']} \mathcal{D}_p^{(i,j)}, \\ \rho &= [\rho_1, \rho_2, \dots, \rho_i, \dots, \rho_{T''}]^T, \\ Y_{sa} &= H(\rho - \frac{1}{T''} \sum_{i=1}^{T''} \rho_i) \in \mathbb{R}^{T''}, \end{aligned} \quad (2)$$

where the superscript T is the transpose operation, and H is a heaviside step function. Furthermore, ρ is the highest similarity of each frame in the anchor video for the positive video, and its average is equal to the positive score (i.e., the video-level similarity between the positive pair), which is

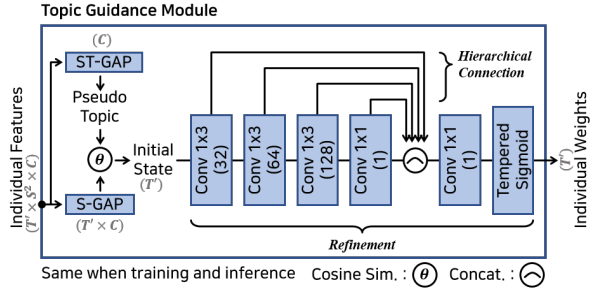


Figure 6: **Pipeline of TGM.** The gray italic letters represent the size of the feature in each process. The number in parentheses in layer blocks indicates the output dimension.

obtained by applying the CS operation to \mathcal{D}_p . The saliency label consists of values where ρ_i is 1 if it is greater than the average of ρ and 0 if it is less, thereby labeling the frame location that significantly contributes to the positive score.

After completing the procedure for creating the saliency label, a self-similarity map is generated by applying TD and CS to two inputs consisting solely of the anchor. The self-similarity map is subsequently fed into the bottleneck layer, the transformer encoder, and the sigmoid to yield saliency weights $W_{sa} = \{w_{sa}^{(t)}\}_{t=1}^{T'}$, as shown in Figure 5. Here, DS is employed to convert to the input of the transformer encoder, and this sequence is inspired by the pipeline of [16]. Consequently, the saliency loss \mathcal{L}_{sa} is computed as the binary cross entropy loss between the saliency weights W_{sa} and the saliency label Y_{sa} , where the nearest interpolation is applied to the label to match the length of the output, T' . The saliency loss \mathcal{L}_{sa} is optimized with the aforementioned frame loss \mathcal{L}_{fr} . During the inference phase, only a self-similarity map for a given target video is fed into the layers to yield saliency weights.

Topic Guidance Module

The extent of suppression for each frame-level feature depends on the topic of the video. For this reason, we create an initial state I that gives direct, video-specific instruction on the topic to help the model generate guidance weights $W_{gu} = \{w_{gu}^{(t)}\}_{t=1}^{T'}$. More specifically, a pseudo-topic G is initially constructed to represent the topic of the video. According to the claim [25] that statistical moments (e.g., mean, max, standard deviation, etc.) have been mathematically proven to be invariant across multiple transformations, the ST-GAP, which consists of average operations, is used to create the pseudo-topic $G \in \mathbb{R}^C$ as a rough representation of the topic that is robust to specific transformations between the frame-level features X . In fact, the topic of a video (even if untrimmed) is determined by what most of the content in that video represents. Therefore, since the average operation yields the direction in which most of the content vectors (i.e., frame-level features) point, an approximate (even if not elaborate) representation of topic can be

obtained. The cosine similarity between the pseudo-topic G and frame-level features X is then employed to build the initial state $I \in \mathbb{R}^{T'}$, which guides the model to reference the topic. At this time, for convenience of operation, the S-GAP is applied to the frame-level features X to remove its spatial axis.

The initial state I is effective in directing the model in a rough pattern along the optimal path to the goal; however, a process of refinement needs to be added with the purpose of providing the guidance weights that more precisely suggest topic relevance. Thus, as illustrated in Figure 6, architecture is designed to refine the coarse pattern. With the initial state I of length T' as input, the data is collected by sliding 1×3 kernels in three convolutional layers, and then a 1×1 convolutional layer reduces the channel dimension. As the preceding three layers are traversed, the receptive field expands, indicating that the temporal spans of data gathered by these layers extend from the short-term to the long-term. Therefore, the output of the preceding three layers and the output of the 1×1 convolutional layer is designed to channel-wise concatenate, which is referred to as a hierarchical connection, to assist the model in grasping the topic relevance of each frame through direct utilization of the knowledge over various temporal spans. After that, a 1×1 convolutional layer is applied to shrink the dimension of the channel axis. Note that only this module employs the tempered sigmoid proposed by [31] rather than the sigmoid to reliably learn the weights from noises that may arise during the refining operation from the rough pattern.

3.6. Video Embedding & Training Strategy

In the training phase, frame-level features are aggregated into a video-level feature $V \in \mathbb{R}^C$ by the Hadamard product with the suppression weights W calculated for each video in a triplet: an anchor, a positive, and a negative. At this time, in the case of positive and negative, only W_{gu} is used as the suppression weights W because their weights are not handled in TSM. As a result, the video loss \mathcal{L}_{vi} is computed as the triplet margin loss between the three video-level features in the triplet. This loss, along with the three losses discussed above, optimizes the model according to Equation (3). In addition, our approach follows the mining scheme of [21] for videos consisting of triplets.

$$\mathcal{L} = \mathcal{L}_{vi} + \mathcal{L}_{fr} + \mathcal{L}_{sa} + \alpha \mathcal{L}_{di} \quad (3)$$

α is a parameter for adjusting the learning of DDM as it is faster than other modules when observed empirically. For reasons of volume limitation, further details are covered in the supplementary material.

	Approach	Dim.	FIVR-200K		
			DSVR	CSVR	ISVR
frame	TN [37]	-	0.724	0.699	0.589
	DP [6]	-	0.775	0.740	0.632
	TCA _{sym} [34]	1,024	0.728	0.698	0.592
	TCA _f [34]	1,024	0.877	0.830	0.703
	Lin <i>et al.</i> [25]	512 ₂₊	0.819	0.764	0.622
	Jo <i>et al.</i> [14]	512 _{2+1,024}	0.896	0.833	0.674
	ViSiL _{sym} [21]	3,840	0.833	0.792	0.654
video	ViSiL _f [21]	3,840	0.843	0.797	0.660
	ViSiL _v [21]	3,840	0.892	0.841	0.702
	HC [35]	-	0.265	0.247	0.193
	DML [23]	500	0.398	0.378	0.309
	TMK [32]	65,536	0.417	0.394	0.319
	LAMV [3]	65,536	0.489	0.459	0.364
	VRAG [30]	4,096	0.484	0.470	0.399
	TCA _c [34]	1,024	0.570	0.553	0.473
	VVS ₅₀₀ (ours)	500	0.606	0.588	0.502
	VVS ₅₁₂ (ours)	512	0.608	0.590	0.505
	VVS ₁₀₂₄ (ours)	1,024	0.645	0.627	0.536
	VVS ₃₈₄₀ (ours)	3,840	0.711	0.689	0.590

Table 1: **Benchmark on FIVR-200K.** The *frame* and *video* refer to frame-level and video-level feature-based approaches. *Dim.* refers to the dimension of the basic unit for calculating similarity in each approach (i.e., frame-level approaches use multiple features of that dimension, as many as the number of all or most frames in a video, while video-level approaches use only one feature of that dimension). The subscript 2 indicates that the feature of that dimension is binarized. Only approaches that are trained from VCDB or do not require additional training are shown for a fair comparison.

4. Experiments

4.1. Evaluation Setup

Our experiments were evaluated on two retrieval settings¹ that is now widely used in content-based video retrieval (CBVR): fine-grained incident video retrieval (FIVR) and near-duplicate video retrieval (NDVR). All performance evaluations are reported based on mean average precision (mAP) [42], and the implementation details are covered in the supplementary material. Furthermore, VCDB [13] is used as a training dataset, and FIVR [20] and CC_WB_VIDEO [40] are used as evaluation datasets.

VCDB is aimed at video copy detection and consists of 528 core datasets with 9,236 partially copied pairs and about 100,000 videos with no additional metadata.

FIVR is equivalent to the FIVR task, which seeks videos connected to certain disasters, occurrences, and incidents. Furthermore, depending on the level of relevance desired, it is evaluated using three criteria: duplicate scene video retrieval (DSVR), complementary scene video re-

¹Some videos from EVVE [33], a dataset for event video retrieval (EVR), another common evaluation setting, could not be downloaded. However, for further comparison, the benchmark for a subset we own ($\approx 70.5\%$ of the original) is covered in the supplementary material.

Approach	Dim.	CC.WEB.VIDEO			
		cc	cc*	cc _c	cc _c *
TN [37]	-	0.978	0.965	0.991	0.987
DP [6]	-	0.975	0.958	0.990	0.982
CTE [7]	-	0.996	-	-	-
TCA _{sym} [34]	1,024	0.982	0.962	0.992	0.981
TCA _f [34]	1,024	0.983	0.969	0.994	0.990
Lin <i>et al.</i> [25]	512 ₂₊	0.972	0.973	0.953	0.976
Jo <i>et al.</i> [14]	512 _{2+1,024}	0.978	0.969	0.983	0.975
ViSiL _{sym} [21]	3,840	0.982	0.969	0.991	0.988
ViSiL _f [21]	3,840	0.984	0.969	0.993	0.987
ViSiL _v [21]	3,840	0.985	0.971	0.996	0.993
HC [35]	-	0.958	-	-	-
DML [23]	500	0.971	0.941	0.979	0.959
VRAG [30]	4,096	0.971	0.952	0.980	0.967
TCA _c [34]	1,024	0.973	0.947	0.983	0.965
VVS₅₀₀ (ours)	500	0.973	0.952	0.981	0.966
VVS₅₁₂ (ours)	512	0.973	0.952	0.981	0.967
VVS₁₀₂₄ (ours)	1,024	0.973	0.952	0.982	0.969
VVS₃₈₄₀ (ours)	3,840	0.975	0.955	0.984	0.973

Table 2: **Benchmark on CC.WEB.VIDEO.** (*) refers to evaluation on the entire dataset, and the subscript *c* refers to the use of cleaned annotations. All other notations and settings are identical to those presented in Table 1.

trieval (CSV), and incident scene video retrieval (ISVR). In this dataset, there are two types in the family: FIVR-5K and FIVR-200K. FIVR-5K has 50 queries and 5,000 videos in the database, while the FIVR-200K has 100 queries and 225,960 videos in the database, both of which have video-level annotations. The FIVR-5K is a subset of the FIVR-200K used for ablation studies, and the FIVR-200K is used for benchmarking as a large-scale video collection.

CC.WEB.VIDEO corresponds to the NDVR task, which aims to find geometrically or photometrically transformed videos. It consists of 13,129 videos in a set of 24 queries and has two types of criteria for evaluation. The criteria are divided into evaluations within each query set or within the entire video, and with the original annotation or the “cleaned” version of the annotation by [21]. The combination of these criteria provides four evaluations.

4.2. Comparison with Other Approaches

Based on the dimension C of a video-level feature V , the proposed approach is referred to as VVS_C . C is equal to that of a frame-level feature X and is determined by dimension reduction during the PCA whitening procedure. If dimension reduction is not applied, it is VVS_{3840} (as used in [21], the dimension of L_N -iMAC is 3840), and if dimension reduction is applied to match the dimension with other approaches, it is VVS_{500} , VVS_{512} and VVS_{1024} .

Table 1 shows comparisons with the previous state-of-the-art on the large-scale dataset, FIVR-200K. In this dataset, VVS_{3840} performs about 25% better than the best video-level approach in all tasks, which is close to the bor-

VVS₃₈₄₀	<i>Elim.</i>		<i>Gen.</i>		FIVR-5K		
	DDM	TSM	TGM	DSVR	CSV	ISVR	
(a)					0.692	0.700	0.651
(b)	✓				0.715	0.725	0.672
(c)		✓			0.703	0.710	0.661
(d)			✓		0.716	0.724	0.677
(e)		✓	✓		0.719	0.726	0.680
(f)	✓	✓			0.724	0.732	0.683
(g)	✓		✓		0.738	0.746	0.698
(h)	✓	✓	✓		0.744	0.752	0.705

Table 3: **Module-wise Ablations for VVS₃₈₄₀.** *Elim.* refers to the easy distractor elimination stage, and *Gen.* refers to the suppression weight generation stage. (a) represents a baseline of the same dimension that weights all frames equally without any of the proposed modules, (b)-(g) represents module-wise ablations, and (h) represents VVS₃₈₄₀.

derline of the frame-level state-of-the-art approaches. In addition, our approaches VVS₅₀₀, VVS₅₁₂ and VVS₁₀₂₄ are state-of-the-art regardless of whether their dimensions match or are smaller than those of other video-level approaches. This trend is similar to the performance on the CC.WEB.VIDEO in Table 2. This proves that our method is the most optimal framework between the two streams, considering that video-level approaches are essentially memory- and speed-efficient.

4.3. Ablation Studies & Analyses

Module-wise Ablations

This section covers ablation studies for each module in the proposed framework VVS₃₈₄₀. As seen in Table 3, each module (b)-(d) demonstrates a significant performance increase over the baseline (a), demonstrating their value. In addition, improvements are observed even when modules are paired with one another (e)-(g), and the same is true when they are all combined (h). Moreover, by presenting further module-wise ablations of VVS₅₀₀, VVS₅₁₂ and VVS₁₀₂₄ in the supplementary material, we show that all modules in our approach have a similar impact.

Component-wise Ablations

This section covers ablation studies for components within each module of the proposed framework.

Distractor Injection Ratio in DDM. Table 4 demonstrates the effect of the sampling ratio from the easy distractor set for injection during the training phase in the DDM. The model can learn slightly more cases for easy distractors compared to a lower ratio when the input length is 20–50% relative to T , leading to enhancements in the overall framework. However, when selected at a higher ratio, the proportion of frames corresponding to the distractor in a video is excessively increased, which hinders optimization.

Existence of Frame Loss in TSM. Table 5 shows the out-

	Injection Ratio	FIVR-5K		
		DSVR	CSVR	ISVR
DDM	0% - 20%	0.739	0.748	0.701
	20% - 50%	0.744	0.752	0.705
	50% - 80%	0.738	0.749	0.704
	80% - 100%	0.728	0.743	0.701

Table 4: **Distractor Injection Ratio in DDM.** This demonstrates the overall impact according to the sampling ratio of the easy distractor set in the DDM.

	Frame Loss \mathcal{L}_{fr}	FIVR-5K		
		DSVR	CSVR	ISVR
TSM		0.742	0.749	0.702
	✓	0.744	0.752	0.705

Table 5: **Existence of Frame Loss \mathcal{L}_{fr} in TSM.** This demonstrates how frame loss affects the TSM.

TGM			FIVR-5K		
Init.	Refine.	Hier.	DSVR	CSVR	ISVR
<i>Rand.</i>	✓	✓	0.693	0.701	0.652
<i>Const.</i>	✓	✓	0.693	0.701	0.652
<i>G</i>			0.625	0.631	0.584
<i>G</i>	✓		0.712	0.722	0.675
<i>G</i>	✓	✓	0.716	0.724	0.677

Table 6: **Structure within TGM.** This demonstrates the impact of the structure within the TGM. *Init.* refers to the initial state I , *Refine.* to the refinement process, and *Hier.* to the hierarchical connection. *Rand.* and *Const.* refer to situations in which the initial state is formed from a random or constant value (which is 0.5), not the pseudo-topic G . To facilitate independent evaluation, the framework excludes all modules except the TGM.

comes of ablation when only the TSM exists with no other modules in order to assess the impact of frame loss on the TSM. In conclusion, the frame loss allows the saliency information to be tuned, resulting in a more exact saliency label and a boost in performance.

Structure within TGM. To test the validity of the TGM structure, ablation studies for each component are shown in Table 6, and all modules other than the TGM are omitted for independent evaluation of each component. First, if random or constant values are used instead of pseudo-topic G while constructing the initial state, performance deteriorates, as the model is implicitly required by relatively unclear criteria rather than explicitly guided by the topic to be well optimized. In addition, the performance gap demonstrates that even with the pseudo-topic, the refinement process with the hierarchical connection is necessary to direct the model appropriately. Furthermore, we reveal in the supplementary material that the hierarchical connection can make the model more robust for various video lengths.

Qualitative Results

Figure 7 depicts the qualitative outcomes produced by the

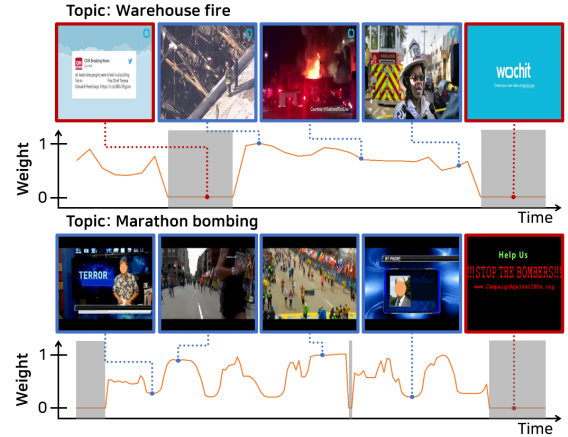


Figure 7: **Qualitative Results on FIVR-5K.** The orange line refers to the weights from the TSM and TGM; the lower the value, the more suppressed the frame. The gray region corresponds to easy distractors eliminated by the DDM, and frames that belong to this area are denoted by a red border.

proposed framework. In the first example, where the topic is “Warehouse fire”, it can be seen that the frames predicted by the DDM as the distractors have few low-level characteristics. In addition, the fourth frame in this example is assigned a relatively low weight because no visual clues directly related to the topic appear. In the second example, where the topic is “Marathon bombing”, it is discovered that frames containing only text and low-level characteristics are deleted by the DDM, as in the first example. Furthermore, among the remaining frames, the weights of those visually related to the topic are measured to be high, whereas the weights of the first and fourth frames, in which the scene of the event does not show directly, are low. From these two examples, it is clear that the proposed approach achieves its intended results.

5. Conclusion

In this paper, we demonstrate that suppression of irrelevant frames is essential in describing an untrimmed video with long and varied content as a video-level feature. And as a solution to this, we presented an end-to-end framework, VVS. It removes frames that can be clearly identified as distractors and determines the degree to which remaining frames should be suppressed based on saliency information and topic relevance. Thus, this is the first approach designed to be learned by explicit criteria, unlike previous approaches that have optimized the model implicitly. Consequently, extensive experiments proved the validity of this design and, at the same time, demonstrated that it is closest to the ideal search scenario among existing approaches due to its competitive speed and efficient memory utilization, as well as its state-of-the-art search accuracy. We hope that this work can contribute to the advancement of real-world video search systems.

References

[1] Call for proposals for compact descriptors for video analysis. *ISO/IEC JTC1/SC29/WG11/N15339*, 2015. 2

[2] Relja Arandjelovic, Petr Gronat, Akihiko Torii, Tomas Pajdla, and Josef Sivic. Netvlad: Cnn architecture for weakly supervised place recognition. In *Proceedings of the IEEE Conference on Computer Vision and Pattern Recognition*, 2016. 1

[3] Lorenzo Baraldi, Matthijs Douze, Rita Cucchiara, and Hervé Jégou. Lamv: Learning to align and match videos with kernelized temporal layers. In *Proceedings of the IEEE Conference on Computer Vision and Pattern Recognition*, 2018. 2, 6

[4] Harry G Barrow, Jay M Tenenbaum, Robert C Bolles, and Helen Cf Wolf. Parametric correspondence and chamfer matching: Two new techniques for image matching. In *Proceedings of Image Understanding Workshop*, 1977. 3

[5] Patrice Bellot and Marc El-Bèze. A clustering method for information retrieval. *Technical Report-0199, Laboratoire d'Informatique d'Avignon, France*, 1999. 1

[6] Chien-Li Chou, Hua-Tsung Chen, and Suh-Yin Lee. Pattern-based near-duplicate video retrieval and localization on web-scale videos. *IEEE Transactions on Multimedia*, 2015. 2, 6, 7, 16

[7] Douze, M., Revaud, J., Verbeek, J., Jégou, H., & Schmid, C. Circulant temporal encoding for video retrieval and temporal alignment. *International Journal of Computer Vision*, 2016. 2, 7

[8] Alan Griffiths, H Claire Luckhurst, and Peter Willett. Using interdocument similarity information in document retrieval systems. *Journal of the American Society for Information Science*, 1986. 1

[9] Geonmo Gu and Byungsoo Ko. Symmetrical synthesis for deep metric learning. In *Proceedings of the AAAI Conference on Artificial Intelligence*, 2020. 1

[10] Kaiming He, Xiangyu Zhang, Shaoqing Ren, and Jian Sun. Deep residual learning for image recognition. In *Proceedings of the IEEE Conference on Computer Vision and Pattern Recognition*, 2016. 11

[11] De-An Huang, Vignesh Ramanathan, Dhruv Mahajan, Lorenzo Torresani, Manohar Paluri, Li Fei-Fei, and Juan Carlos Niebles. What makes a video a video: Analyzing temporal information in video understanding models and datasets. In *Proceedings of the IEEE Conference on Computer Vision and Pattern Recognition*, 2018. 13

[12] Hervé Jégou and Ondřej Chum. Negative evidences and co-occurrences in image retrieval: The benefit of pca and whitening. In *European Conference on Computer Vision*, 2012. 3

[13] Yu-Gang Jiang, Yudong Jiang, and Jiajun Wang. Vcdb: a large-scale database for partial copy detection in videos. In *European Conference on Computer Vision*, 2014. 6, 11, 13

[14] Won Jo, Guentaek Lim, Joonsoo Kim, Joungil Yun, and Yukyung Choi. Exploring the temporal cues to enhance video retrieval on standardized cdva. *IEEE Access*, 2022. 1, 2, 6, 7, 17

[15] HeeJae Jun, Byungsoo Ko, Youngjoon Kim, Insik Kim, and Jongtack Kim. Combination of multiple global descriptors for image retrieval. *arXiv preprint arXiv:1903.10663*, 2019. 1

[16] Hyolim Kang, Jinwoo Kim, Taehyun Kim, and Seon Joo Kim. Uboco: Unsupervised boundary contrastive learning for generic event boundary detection. In *Proceedings of the IEEE Conference on Computer Vision and Pattern Recognition*, 2022. 3, 5

[17] Diederik P Kingma and Jimmy Ba. Adam: A method for stochastic optimization. *arXiv preprint arXiv:1412.6980*, 2014. 11

[18] Byungsoo Ko and Geonmo Gu. Embedding expansion: Augmentation in embedding space for deep metric learning. In *Proceedings of the IEEE Conference on Computer Vision and Pattern Recognition*, 2020. 1

[19] Byungsoo Ko, Minchul Shin, Geonmo Gu, HeeJae Jun, Tae Kwan Lee, and Youngjoon Kim. A benchmark on tricks for large-scale image retrieval. *arXiv preprint arXiv:1907.11854*, 2019. 1

[20] Giorgos Kordopatis-Zilos, Symeon Papadopoulos, Ioannis Patras, and Ioannis Kompatsiaris. Fivr: Fine-grained incident video retrieval. *IEEE Transactions on Multimedia*, 2019. 6, 13

[21] Giorgos Kordopatis-Zilos, Symeon Papadopoulos, Ioannis Patras, and Ioannis Kompatsiaris. Visil: Fine-grained spatio-temporal video similarity learning. In *Proceedings of IEEE Conference on Computer Vision*, 2019. 1, 2, 3, 4, 5, 6, 7, 16, 17

[22] Giorgos Kordopatis-Zilos, Symeon Papadopoulos, Ioannis Patras, and Yiannis Kompatsiaris. Near-duplicate video retrieval by aggregating intermediate cnn layers. In *Proceedings of International Conference on Multimedia Modeling*, 2017. 2

[23] Giorgos Kordopatis-Zilos, Symeon Papadopoulos, Ioannis Patras, and Yiannis Kompatsiaris. Near-duplicate video retrieval with deep metric learning. In *Proceedings of IEEE Conference on Computer Vision Workshops*, 2017. 1, 2, 3, 6, 7, 12, 16, 17

[24] Giorgos Kordopatis-Zilos, Christos Tzelepis, Symeon Papadopoulos, Ioannis Kompatsiaris, and Ioannis Patras. Dns: Distill-and-select for efficient and accurate video indexing and retrieval. *International Journal of Computer Vision*, 2022. 2

[25] Jie Lin, Ling-Yu Duan, Shiqi Wang, Yan Bai, Yihang Lou, Vijay Chandrasekhar, Tiejun Huang, Alex Kot, and Wen Gao. Hnlp: Compact deep invariant representations for video matching, localization, and retrieval. *IEEE Transactions on Multimedia*, 2017. 2, 5, 6, 7, 17

[26] Min Lin, Qiang Chen, and Shuicheng Yan. Network in network. *arXiv preprint arXiv:1312.4400*, 2013. 3

[27] Ling-Yu Duan, Yan Bai, Vijay Chandrasekhar, Tiejun Huang, Shiqi Wang, Alex Chichung Kot, Yihang Lou, Wen Gao, Jie Lin. Compact descriptors for video analysis: The emerging mpeg standard. *IEEE MultiMedia*, 2018. 2

[28] Xiaoyong Liu and W Bruce Croft. Cluster-based retrieval using language models. In *Proceedings of the 27th annual international ACM SIGIR conference on Research and development in information retrieval*, 2004. 1

[29] Yihang Lou, Yan Bai, Jie Lin, Shiqi Wang, Jie Chen, Vijay Chandrasekhar, Ling-Yu Duan, Tiejun Huang, Alex Chichung Kot, and Wen Gao. Compact deep invariant descriptors for video retrieval. In *Proceedings of Data Compression Conference*, 2017. 2

[30] Kennard Ng, Ser-Nam Lim, and Gim Hee Lee. Vrag: Region attention graphs for content-based video retrieval. *arXiv preprint arXiv:2205.09068*, 2022. 1, 2, 3, 6, 7, 11, 12, 16, 17

[31] Nicolas Papernot, Abhradeep Thakurta, Shuang Song, Steve Chien, and Úlfar Erlingsson. Tempered sigmoid activations for deep learning with differential privacy. In *Proceedings of the AAAI Conference on Artificial Intelligence*, 2021. 6, 11, 14

[32] Sébastien Poullot, Shunsuke Tsukatani, Anh Phuong Nguyen, Hervé Jégou, and Shin’Ichi Satoh. Temporal matching kernel with explicit feature maps. In *Proceedings of ACM International Conference on Multimedia*, 2015. 2, 6, 16

[33] Jérôme Revaud, Matthijs Douze, Cordelia Schmid, and Hervé Jégou. Event retrieval in large video collections with circulant temporal encoding. In *Proceedings of the IEEE Conference on Computer Vision and Pattern Recognition*, 2013. 6, 17

[34] Jie Shao, Xin Wen, Bingchen Zhao, and Xiangyang Xue. Temporal context aggregation for video retrieval with contrastive learning. In *Proceedings of IEEE Winter Conference on Applications of Computer Vision*, 2021. 1, 2, 3, 6, 7, 12, 16, 17

[35] Jingkuan Song, Yi Yang, Zi Huang, Heng Tao Shen, and Jiebo Luo. Effective multiple feature hashing for large-scale near-duplicate video retrieval. *IEEE Transactions on Multimedia*, 2013. 2, 6, 7

[36] Tomek Strzalkowski. Natural language information retrieval. *Information Processing & Management*, 1995. 1

[37] Hung-Khoon Tan, Chong-Wah Ngo, Richard Hong, and Tat-Seng Chua. Scalable detection of partial near-duplicate videos by visual-temporal consistency. In *Proceedings of ACM International Conference on Multimedia*, 2009. 2, 6, 7, 16

[38] Giorgos Tolias, Ronan Sicre, and Hervé Jégou. Particular object retrieval with integral max-pooling of cnn activations. In *Proceedings of International Conference on Learning Representations*, 2016. 1, 3

[39] Petar Veličković, Guillem Cucurull, Arantxa Casanova, Adriana Romero, Pietro Lio, and Yoshua Bengio. Graph attention networks. *arXiv preprint arXiv:1710.10903*, 2017. 3

[40] Xiao Wu, Chong-Wah Ngo, Alexander G Hauptmann, and Hung-Khoon Tan. Real-time near-duplicate elimination for web video search with content and context. *IEEE Transactions on Multimedia*, 2009. 6

[41] Yongxin Yang and Timothy Hospedales. Deep multi-task representation learning: A tensor factorisation approach. *arXiv preprint arXiv:1605.06391*, 2016. 3

[42] Mu Zhu. Recall, precision and average precision. *Department of Statistics and Actuarial Science, University of Waterloo, Waterloo*, 2004. 6

VVS: Video-to-Video Retrieval with Irrelevant Frame Suppression

-Supplementary Material-

In this supplementary material, we offer extra information to supplement the main script. Appendix A focuses mainly on details. Appendix A.1 offers the implementation details of the proposed framework, and Appendix A.2 discusses the training strategy details. Appendix A.3 covers formulas details of the losses to train our approach, and Appendix A.4 provides architecture details via detailed pipelines. Appendix B focuses mainly on additional ablation studies and analyses. As stated in the introduction of the main script, Appendix B.1 explains the quantitative experiment indicating that the description of video-level features with optimal suppression of irrelevant frames can be an ideal retrieval scenario. Appendix B.2 offers examples within the easy distractor set and describes the configuration process of the set. Appendix B.3 discusses the advantages of using the tempered sigmoid rather than the sigmoid in our approach. As stated in the main script while introducing TSM, Appendix B.4 reveals that saliency information (i.e., saliency signals) can enhance the representation of video-level features. Appendix B.5 demonstrates why TGM, a module within the proposed framework, includes the refinement process via the hierarchical connection. Appendix B.6 includes numerical comparisons between the proposed approach and other approaches in terms of speed and memory. Appendix B.7 provides an additional benchmark for the subset of the EVVE dataset for the reasons stated in the evaluation setup footnote of the main script. Appendix B.8 addresses further module-wise ablations for the proposed approaches: VVS₅₀₀, VVS₅₁₂, and VVS₁₀₂₄. Appendix B.9 contains numerous qualitative results of the proposed framework.

A. Additional Details

A.1. Implementation Details

Each video is sampled at one frame per second. The number of frames per video is set during training with $T = 64$ but is varied during inference based on the duration of the video. In the L_N -iMAC, the backbone network Φ is ResNet50 [10], the number of layers K is 4, the types of

region kernel N are 4. The set of easy distractors used in the training phase is taken from nearly 100,000 metadata-free videos (with the exception of 528 videos in the core datasets) within the VCDB [13], where each frame-level feature is selected as an easy distractor based on the magnitude threshold $\lambda_{mag} = 40$. The distractor threshold λ_{di} for the thresholding operation on the confidence of DDM during the inference phase is set to 0.5. The temperature of the tempered sigmoid [31] is set to 512 in TGM. The parameter α for balancing the discrimination loss is set to 0.5, and margins in the frame loss and the video loss are also set to 0.5. Additionally, PCA is incrementally trained from all metadata-free videos within the VCDB.

All experiment code is implemented with Pytorch on an NVIDIA Tesla V100. To achieve reasonable time comparisons throughout the inference phase, all speed-related experiments are measured synchronously. Given that the CUDA call from Pytorch is fundamentally asynchronous, this synchronous measurement prevents erroneous measurements of overall operating time on the CPU and GPU. In addition, the total inference time includes model operation time, similarity calculation time, and evaluation time after extracting frame-level features, as in [30].

Experiments that are not explicitly indicated (e.g., VVS₅₀₀, VVS₅₁₂, or VVS₁₀₂₄) in the main script and supplementary material were all conducted using VVS₃₈₄₀.

A.2. Training Strategy Details

The proposed approach is learned through the Adam [17] optimizer with one batch, and a fixed learning rate of 2×10^{-5} , during 60 epochs using 2,000 iterations. The best model during these epochs is chosen using mAP on the FIVR-5K, considered a validation set in this field of study. In addition, videos from the VCDB, including the core dataset and metadata-free videos, are sampled during the training phase to form a triplet.

Furthermore, easy distractors injected into an input of DDM are derived from metadata-free videos. For this reason, only frame-level features chosen from the core dataset, except metadata-free videos, are used as the input of DDM

for learning. Specifically, if an input is provided from metadata-free videos, DDM is trained by injecting easy distractors into the input and then creating a pseudo-label based on the position of the injected distractors. However, before the easy distractors are injected, frames included in the easy distractor set may already exist in the input. Therefore, even if specific frames are included in the set of easy distractors, the pseudo-label may state that they are not easy distractors. Consequently, to avoid confusion during model optimization, DDM is trained solely on frame-level features from the core dataset, with the exception of those from metadata-free videos used to generate the easy distractor set. In addition, unlike other modules, DDM takes frame-level features without PCA as input to directly assess to what extent layers of the backbone network activate low-level characteristics.

A.3. Formulas Details

This section covers the details of the formulas for each loss, which are omitted in the main script due to their already well-known forms, to help readers understand our approach.

Discrimination Loss

The discrimination loss \mathcal{L}_{di} is the form of the binary cross entropy loss between the confidence $W_{di} = \{w_{di}^{(t)}\}_{t=1}^{T'}$ and the pseudo-label $Y_{di} = \{y_{di}^{(t)}\}_{t=1}^{T'}$ obtained from DDM to identify easy distractors, which can be formulated as follows:

$$\mathcal{L}_{di} = \frac{1}{T'} \sum_{t=1}^{T'} y_{di}^{(t)} \log(w_{di}^{(t)}) + (1 - y_{di}^{(t)}) \log(1 - w_{di}^{(t)}). \quad (\text{i})$$

Frame Loss

The frame loss \mathcal{L}_{fr} , which calibrates saliency information in TSM, is the sum of the triplet margin loss for tuned similarity maps and the regularization loss. The triplet margin loss (denoted by \mathcal{L}_{tri}) is the form of the well-known triplet margin loss between the tuned similarity maps \mathcal{D}_p and \mathcal{D}_n for the positive and negative pair calculated within TSM, which can be formulated as follows:

$$\mathcal{L}_{tri} = \max \{0, CS(\mathcal{D}_n) - CS(\mathcal{D}_p) + \gamma\}, \quad (\text{ii})$$

where γ is the margin. The regularization loss (denoted by \mathcal{L}_{reg}) is a form of divergence constraint between the two tuned similarity maps \mathcal{D}_p and \mathcal{D}_n , which can be formulated as follows:

$$\begin{aligned} \psi(\mathcal{D}) &= \sum |\max \{0, \mathcal{D} - J\}| + |\min \{0, \mathcal{D} + J\}|, \\ \mathcal{L}_{reg} &= \psi(\mathcal{D}_p) + \psi(\mathcal{D}_n), \end{aligned} \quad (\text{iii})$$

where 0 and J are matrices of zeros and ones with the same size as \mathcal{D}_p and \mathcal{D}_n . Consequently, the frame loss \mathcal{L}_{fr} is

the form of the weighted sum between the two prior losses, which can be formulated as follows:

$$\mathcal{L}_{fr} = \mathcal{L}_{tri} + 0.5 * \mathcal{L}_{reg}. \quad (\text{iv})$$

Saliency Loss

The saliency loss \mathcal{L}_{sa} is the form of the binary cross entropy loss between the saliency weights $W_{sa} = \{w_{sa}^{(t)}\}_{t=1}^{T'}$ and the saliency label $Y_{sa} = \{y_{sa}^{(t)}\}_{t=1}^{T'}$ obtained from TSM to assess the significance of each frame, which can be formulated as follows:

$$\mathcal{L}_{sa} = \frac{1}{T'} \sum_{t=1}^{T'} y_{sa}^{(t)} \log(w_{sa}^{(t)}) + (1 - y_{sa}^{(t)}) \log(1 - w_{sa}^{(t)}). \quad (\text{v})$$

Video Loss

The video loss \mathcal{L}_{vi} is the form of the triplet margin loss between video-level features within a triplet, which can be formulated as follows:

$$\mathcal{L}_{vi} = \max \{0, \theta(V, V^-) - \theta(V, V^+) + \gamma\}, \quad (\text{vi})$$

where V , V^+ , and V^- are video-level features derived from an anchor, a positive, and a negative within the triplet; $\theta(\cdot)$ is the cosine similarity; and γ is the margin.

Since our approach is simultaneously optimized from all the losses described above, we term it the “end-to-end framework” to avoid the misunderstanding that each stage is learned individually (in practice, two stages are trained at once); however, note that the backbone network for extracting L_N -iMAC remains frozen, as is usual in this line of research.

A.4. Architecture Details

This section gives more details on the pipelines depicted in the main script to facilitate reproducibility and comprehension of the proposed system. These details describe the size of the data traveling through the pipeline in each module as well as the parameters for each layer. Figure G describes the detailed pipeline for the overall framework, Figure H for DDM, Figure I for TSM, and Figure J for TGM.

B. Additional Ablation Studies & Analyses

B.1. Quantitative Experiment on Ideal Suppression

In this section, we demonstrate an ideal experiment to highlight the value of suppressing irrelevant frames when describing distinct video-level features. Concretely, the purpose of this experiment is to reveal how much previous approaches [23, 34, 30] can profit from manually eliminating frames corresponding to distractors in their scheme. The

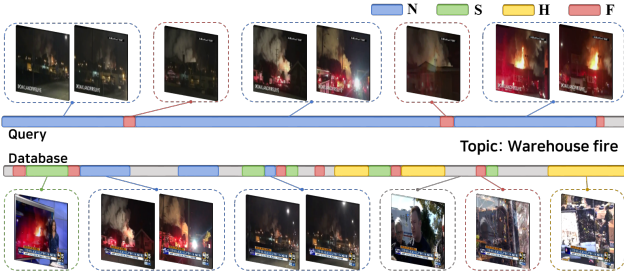


Figure A: Example of Temporal Annotation for FIVR-5K. This example illustrates the temporal annotations for a topic-related pair within FIVR-5K. N, S, H, and F represent segment-level labels for the related areas of the pair. N refers to segments where the temporal span and camera viewpoint are similar; S refers to segments where the temporal span is similar but the camera viewpoint is different; H refers to segments where the temporal span and camera viewpoint are different, but it can be inferred semantically as the same topic; and F refers to segments where a fading effect is observed before or after the segments corresponding to the preceding labels. Note that the temporal annotations are not proposed in this submission but will be released soon.

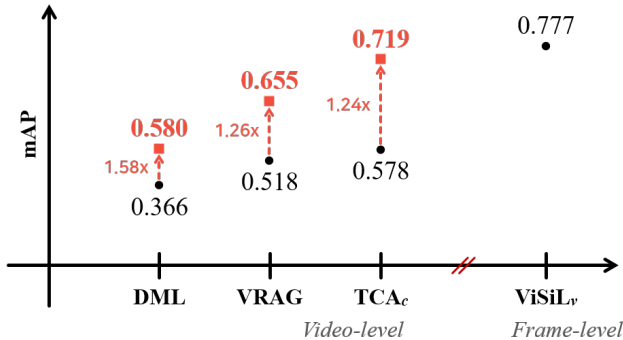


Figure B: Oracle of Previous Approaches on FIVR-5K. This indicates that proper suppression is key for the ideal video-level scheme. All performances are measured in the ISVR of FIVR-5K, with black circles representing the original performances of earlier approaches and red squares the performances after irrelevant frames are manually eliminated.

experiment is performed on the FIVR-5K [20] using temporal annotations to erase distractors. As depicted in Figure A, the temporal annotations comprise segment-level labels indicating which areas of each video are related to one another for a topic-related pair between query and database in the FIVR-5K. The segment-level labels consist of three types: N, S, and H; the closer to N, the more visually related; and the closer to H, the more semantically related. In addition, this annotation also includes label F, indicating that the fade effect occurred before and after the three preceding labels. The remaining regions, excluding N, S, and H, are presumed to be distractors because they contain

Magnitude Interval	Cumulative Percentage
- 20	1.15%
20 - 30	2.61%
30 - 40	8.96%
40 - 50	25.19%
50 - 60	61.46%
60 -	100.00%

Table A: Percentage by Magnitude Interval on VCDB. This is the cumulative percentage by interval of the magnitude of all frame-level features derived from metadata-free videos within the VCDB. “- 20” refers to an interval whose magnitude is less than 20, and “60 -” refers to 60 or higher.

irrelevant content to the topic or may cause confusion owing to the fade effect. As a consequence, for a total of 1,981 videos with the temporal annotations inside the FIVR-5K, video-level features are described while removing frames from locations identified as distractors in the scheme of earlier approaches. Note that 3,069 videos without the temporal annotations are handled in the original manner. Because this experiment employs the temporal annotations directly for prediction, it involves “cheating” and cannot be used as a benchmark. However, it provides a glimpse of the upper bound for existing approaches when optimal suppression is possible; it is dubbed Oracle, the same as in [11].

Figure B shows the ISVR performance on FIVR-5K for the earlier video-level feature-based approaches obtained through the experiment stated above, i.e. the Oracle. All cases when the temporal annotations are employed for ideal suppression are enhanced by 1.24 times at least and 1.58 times at most. In particular, the search accuracy, which has been recognized as a weakness of video-level approaches, is close to that of the most advanced frame-level approach (ViSiL_v), implying that a scenario capable of fast and accurate response can be reached if only inappropriate frames are excluded when describing video-level features.

B.2. Examples within Easy Distractor Set

This section discusses the easy distractor set used for DDM training. The easy distractor set is derived from metadata-free videos in the training dataset VCDB [13], as stated in the main script. Specifically, L_N-iMAC, which are frame-level features, are extracted from all of these videos, but PCA are not applied in order to assess directly to what extent layers of the backbone network activate low-level characteristics. After that, their magnitude is filtered by the magnitude threshold λ_{mag} ; if this value is less than the threshold, the frame is added to the easy distractor set. The reason for identifying easy distractors in this criterion is that

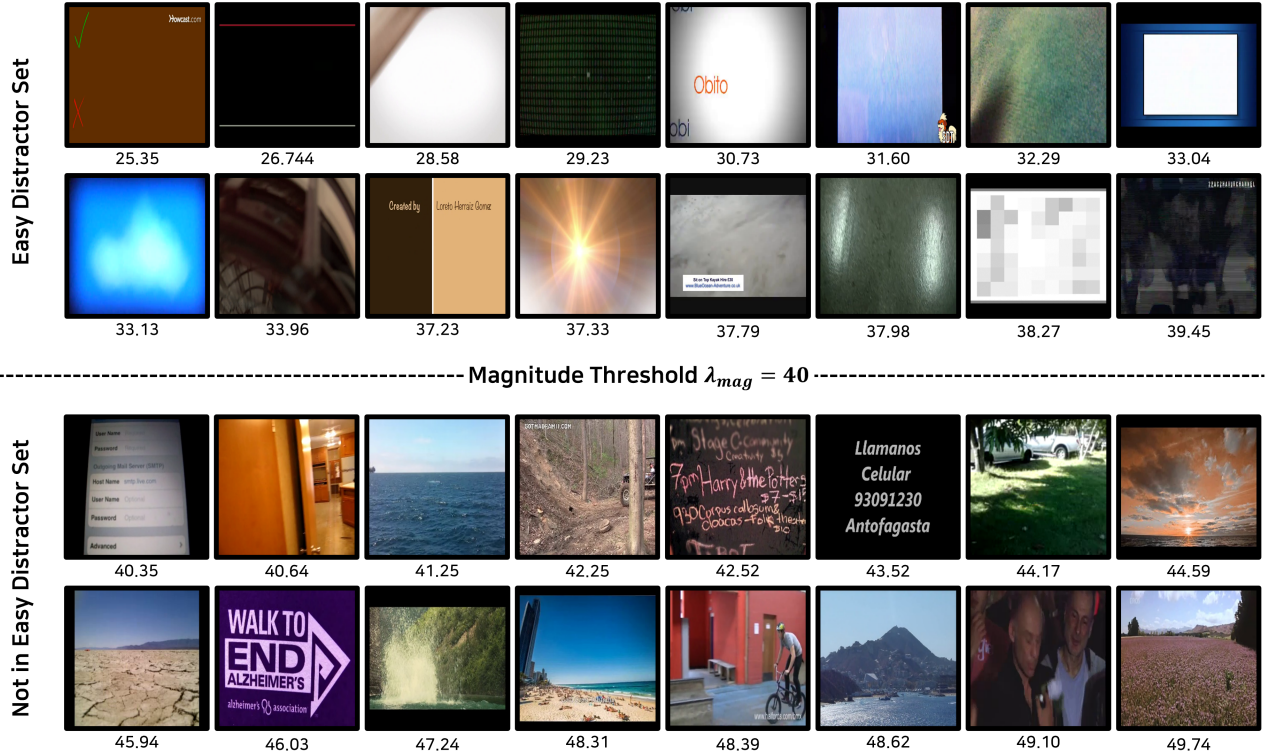


Figure C: Example of Per-Frame Magnitude for Easy Distractor Selection on VCDB. This represents the magnitude of frame-level features (L_N -iMAC) belonging to the metadata-free videos within the training dataset VCDB. The letters under each frame indicate its magnitude.

fewer low-level characteristics and smaller pixel variations result in fewer elements being activated in the process of describing frame-level features, leading to a smaller scale of output elements. However, if filtering is performed with a magnitude threshold that is too small for a perfect easy distractor, the variance within the set of easy distractors is reduced, leading to overfitting of the pattern of a particular easy distractor. In contrast, if filtering is conducted with a value that is too high, many frames will be deemed to be the easy distractor and eliminated by DDM, despite the fact that they may include several signals for topic comprehension. To select an appropriate magnitude threshold value in this trade-off relationship, the magnitudes of all frame-level features are categorized by interval and converted to cumulative percentages, as shown in Table A. As a result, the magnitude threshold is set to 40 (corresponding to “30-40”), considering that the cumulative amount of the interval is a sufficient proportion close to 10% of the total training data before the cumulative percentage exploded rapidly. In addition, the appropriateness of this value is illustrated with qualitative examples in Figure C; in fact, when the magnitude threshold is less than 40, it is evident that the major-

ity of frames are assessed as easy distractors. Even though there are frames that can be identified as easy distractors when the magnitude threshold is more than 40, there are also numerous landscapes that may be used to depict the topic of a certain video, demonstrating that the magnitude threshold currently in use is a well-balanced value.

B.3. Advantages of Tempered Sigmoid

This section discusses why the tempered sigmoid is used instead of the sigmoid only in TGM. The tempered sigmoid [31] was proposed in order to provide robustness to noise in the training phase by controlling the gradient norm, which can be formulated as follows:

$$\omega(h) = \frac{\sigma}{1 + e^{-h/\tau}} - o \quad (vii)$$

where ω refers to the tempered sigmoid function, σ to a parameter that controls the activation scale, τ to the temperature that reduces the gradient norm so that model parameters can be updated carefully, and o to the offset.

In fact, TGM receives as input the output of DDM, which comprises injected easy distractors as well as topic-related and topic-unrelated content that originally existed in an in-

Tempered Sigmoid			FIVR-5K		
DDM	TSM	TGM	DSVR	CSVR	ISVR
			0.727	0.744	0.701
✓	✓	✓	0.728	0.739	0.694
			0.737	0.743	0.696
			0.744	0.752	0.705
✓	✓	✓	0.733	0.740	0.695

Table B: **Effect of Tempered Sigmoid on Each Module.** If a check mark is present, it indicates that the tempered sigmoid replaces the sigmoid of that module.

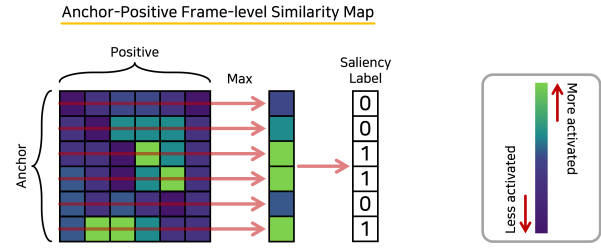
put video. As the ST-GAP, a global operation, is applied to the input of TGM to obtain the rough pattern, noise has a greater impact on optimization than other modules. Therefore, the tempered sigmoid with the aforementioned benefits is utilized to train TGM more stably. Here, σ and o are set to 1 and 0 because the result of the tempered sigmoid is utilized guidance weights, which have values between 0 and 1. Also, τ is empirically set to 512.

As seen in Table B, when the tempered sigmoid is used instead of the sigmoid solely for TGM, the performance of the ISVR increases from 0.701 to 0.705 compared to when the tempered sigmoid is not employed anywhere. However, as other modules besides TGM have a relatively low emerging chance of noise, a small gradient norm caused by the tempered sigmoid only results in insufficient optimization.

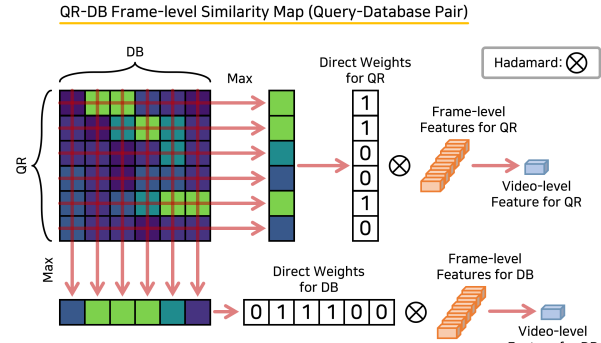
B.4. Effect of Saliency Signal on Representation

In TSM, the model is guided by a pseudo-label, i.e., a saliency label, generated based on saliency signals (also referred to as saliency information) within a frame-level similarity map. This section covers a direct interpretation of whether these saliency signals actually contribute to the representation of video-level features.

To verify the contribution of saliency signals to the representation, direct weights obtained from a frame-level similarity map are employed during the inference phase. The process begins with the baseline (referred to in the module-wise ablation studies of VVS₃₈₄₀ presented in the main script), in which all frame-level features are aggregated with the same weights without any of the proposed modules. Technically, before describing a video-level feature, as shown in (b) of Figure D, a frame-level similarity map is computed for each pair consisting of one query and one video within the database. Here, the map is identical to when acquiring a saliency label, i.e., it is a finely tuned map. The maximum operation is then applied to the map and converted to 1 or 0, which is also the same as obtaining a saliency label (this process is illustrated in (a) of Figure D),



(a) Process for Calculating Saliency Label



(b) Process for Calculating Direct Weights

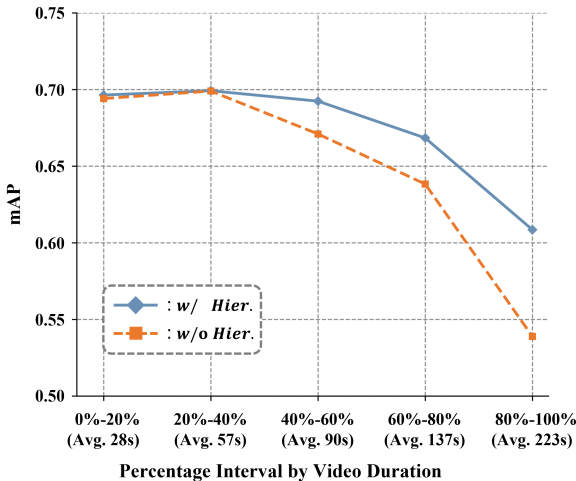
Figure D: **Toy Example for Direct Weights.** This simplifies the calculation process of direct weights for demonstrating the effect of saliency signals on video-level feature representation, as discussed in Appendix B.4, in comparison to the calculation process of saliency label.

	FIVR-5K		
	DSVR	CSVR	ISVR
(a)	0.692	0.700	0.651
(b)	0.799	0.799	0.726

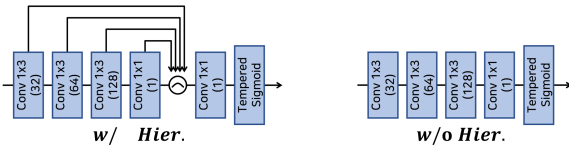
Table C: **Effect of Saliency Signal on Representation.** (a) represents the baseline (referred to in the module-wise ablation studies of VVS₃₈₄₀ presented in the main script) that weights all frames equally without any of the proposed modules. (b) represents the scenario when direct weights are employed at the baseline, as stated in Appendix B.4.

but the outcome here corresponds to direct weights for the query. In addition, similar to this procedure, the maximum operation is applied in an orthogonal direction to produce direct weights for the video within the database. After that, a video-level feature for each video is aggregated by using the Hadamard product between the frame-level features of each video and the direct weights for that video.

This verification procedure cannot be termed a “video-level approach” because the similarities are computed first



(a) Performance over Duration on FIVR-5K



(b) Structural Difference of TGM by Hierarchical Connection

Figure E: Effect of Hierarchical Connection. This demonstrates the merit of hierarchical connection within the TGM according to various video durations on FIVR-5K. In (a), the horizontal axis indicates that each of the five subsets into which the FIVR-5K database is divided based on the duration interval replaces the entire database. In other words, 0%-20% is a case where only one-fifth of the database is used in the order of shorter duration in the database, and 80%-100% is a case in the order of longer duration. Furthermore, the average duration of the videos included in each interval is indicated in parentheses below each one. The vertical axis represents mAP in ISVR, and *Hier.* refers to the hierarchical connection. A blue solid line indicates when the hierarchical connection exists, while an orange dashed line indicates when it does not. The structural difference in TGM resulting from the presence of hierarchical connection can be seen in (b).

from frame-level features in order to create the direct weights during the inference phase. However, this procedure allows one to figure out to what extent saliency signals can help describe video-level features. Because the direct weights for the query and the video within the database, which are formed in the same manner as a saliency label, are directly engaged in aggregating video-level features.

As shown in Table C, when direct weights are employed (b), significant performance increases are found over the baseline (a), indicating that saliency signals are strongly linked to strengthening the representation of video-level

	Approach	Dim.	Inference Time (sec/q)	# of Features
frame	DP [6]	-	137.57s	
	TN [37]	-	3.61s	
	ViSiL _{sym} [21]	3,840	8.24s	
	ViSiL _v [21]	3,840	8.16s	540,361
	ViSiL _f [21]	3,840	3.76s	
	TCA _{sym} [34]	1,024	4.00s	
video	TCA _f [34]	1,024	2.14s	
	TMK [32]	65,536	7.23s	
	VRAG [30]	4,096	0.79s	
	DML [23]	500	0.61s	
	TCA _c [34]	1,024	0.28s	5,000
	VVS₅₀₀ (ours)	500	0.57s	
	VVS₅₁₂ (ours)	512	0.58s	
	VVS₁₀₂₄ (ours)	1,024	0.59s	
	VVS₃₈₄₀ (ours)	3,840	0.64s	

Table D: Inference Time & Number of Features. This demonstrates the average inference seconds per query on the FIVR-5K and the number of those database features that need to be stored in memory. The *frame* and *video* refer to frame-level and video-level feature-based approaches. *Dim.* refers to the dimension of the basic unit for calculating similarity in each approach (i.e., frame-level approaches use multiple features of that dimension, as many as the number of all or most frames in a video, while video-level approaches use only one feature of that dimension).

features. Moreover, the results in that table demonstrate that the saliency label in TSM mainly leads the model to explore visual correlations, as the improvements in the DSVR task, where discovering visually related scenes is a priority, are greater than in other tasks.

B.5. Effect of Hierarchical Connection on TGM

This section explains the effectiveness of leveraging the hierarchical connection in TGM. To recap what was discussed in the main script, the hierarchical connection is a strategy to assist the model in grasping the topic by directly utilizing data that covers different temporal spans caused by multiple convolution layers in the refinement process. This direct use of knowledge on various temporal spans is intended to help understand the content of varying lengths included in videos, and it can be expected that this strategy will be more beneficial for longer videos, which have more content.

In fact, the experiment represented in (a) of Figure E demonstrates that the expectation is satisfied. The experiment is conducted by splitting the full database such that it contains just videos of a particular duration interval and evaluating the effect of hierarchical connection on that duration interval. Specifically, the FIVR-5K database is separated into five subsets of the same amount based on the dura-

Approach	Dim.	EVVE															
		Avg.	#1	#2	#3	#4	#5	#6	#7	#8	#9	#10	#11	#12	#13		
frame	Lin <i>et al.</i> [25]	512 ₂₊	512	0.484	0.770	0.588	0.334	0.243	0.307	0.270	0.225	0.145	0.337	0.318	0.060	0.797	0.234
	Jo <i>et al.</i> [14]	512 ₂ +1,024		0.559	0.749	0.602	0.315	0.318	0.355	0.316	0.336	0.229	0.302	0.462	0.176	0.843	0.645
	TCA _f [34]		1,024	0.636	0.885	0.698	0.251	0.449	0.395	0.390	0.289	0.271	0.583	0.666	0.338	0.893	0.829
	ViSiL _f [21]		3,840	0.585	0.834	0.625	0.148	0.427	0.347	0.355	0.277	0.183	0.355	0.586	0.296	0.860	0.747
	ViSiL _{sym} [21]		3,840	0.646	0.858	0.775	0.434	0.399	0.418	0.298	0.371	0.295	0.698	0.583	0.315	0.930	0.762
video	ViSiL _v [21]		3,840	0.659	0.919	0.810	0.360	0.421	0.405	0.360	0.298	0.278	0.567	0.667	0.391	0.929	0.827
	DML [23]		500	0.541	0.414	0.461	0.082	0.233	0.315	0.300	0.259	0.170	0.078	0.470	0.274	0.883	0.705
	TCA _c [34]		1,024	0.599	0.687	0.591	0.154	0.390	0.357	0.381	0.288	0.264	0.544	0.615	0.272	0.871	0.790
	VRAG [30]		4,096	0.632	0.772	0.705	0.104	0.283	0.370	0.311	0.286	0.302	0.610	0.701	0.371	0.918	0.762
	VVS₅₀₀ (ours)		500	0.629	0.732	0.659	0.210	0.398	0.351	0.409	0.292	0.274	0.588	0.684	0.343	0.904	0.811
	VVS₅₁₂ (ours)		512	0.630	0.733	0.654	0.206	0.413	0.353	0.416	0.289	0.273	0.611	0.689	0.348	0.903	0.812
	VVS₁₀₂₄ (ours)		1,024	0.630	0.763	0.669	0.168	0.396	0.360	0.401	0.304	0.285	0.516	0.683	0.353	0.902	0.807
	VVS₃₈₄₀ (ours)		3,840	0.644	0.835	0.731	0.210	0.433	0.375	0.423	0.325	0.282	0.423	0.667	0.403	0.910	0.840

Table E: **Benchmark on EVVE.** The results are reported on a subset we own ($\approx 70.5\%$ of the original) using the trained model provided by the official code of each approach due to the unavailability of the full original dataset. The *frame* and *video* refer to frame-level and video-level feature-based approaches. *Dim.* refers to the dimension of the basic unit for calculating similarity in each approach (i.e., frame-level approaches use multiple features of that dimension, while video-level approaches use only one feature of that dimension). The subscript 2 indicates that the feature of that dimension is binarized. #1 through #13 refer to the mAP of the event corresponding to the id listed in [33], and Avg. refers to the mAP for all events. Only approaches that are trained from VCDB or do not require additional training are shown for a fair comparison.

tion order. The search performance is then evaluated using each subset as a database. At this time, the performances over the duration interval are measured for the presence or absence of the hierarchical connection. Furthermore, their structural difference can be seen in (b) of Figure E. Consequently, the longer videos, the higher the performances when the hierarchical connection is present as opposed to when it is not. This suggests that, in accordance with the design intent of the hierarchical connection, the direct integration over multiple temporal spans in lengthy videos with several contents of varying durations aids comprehension of the topic.

B.6. Efficiency on Speed and Memory

Table D demonstrates that the video-level feature-based approach is much faster than the frame-level approach in terms of average inference seconds per query and that, regardless of dimensions, our approach is at least 3.3 times faster than the fastest frame-level approach (TCA_f) on the FIVR-5K. Furthermore, video-level approaches like ours store about 108 times (this ratio increases as average duration in the dataset increases) less on this dataset. This is quite memory efficient considering the actual scenario in which the database features are stored in advance in memory to facilitate the processing of queries transmitted in real time. In summary, this section demonstrates that our approach, which is close to the accuracy of frame-level approaches as presented in the main script, is also competitive

in terms of speed and memory efficiency, which are the primary characteristics of video-level approaches.

B.7. Comparison with Other Approaches on EVVE

Table E shows comparisons with earlier approaches on the EVVE [33], a dataset for event video retrieval (EVR). Note that several videos in the original dataset were missing; however, the benchmark is presented on the subset we own ($\approx 70.5\%$ of the original) for further comparison on a dataset considered more challenging.

Despite having fewer dimensions, VVS₃₈₄₀ outperforms VRAG [30], which represents the state-of-the-art performance among current video-level approaches. This performance is better than the majority of the frame-level state-of-the-art. Furthermore, VVS₅₀₀, VVS₅₁₂ and VVS₁₀₂₄ with dimension reduction during the PCA procedure surpass the video-level approach of the same dimension in every case.

B.8. Further Module-wise Ablations

This section covers further ablation studies for each module in the proposed framework: VVS₅₀₀, VVS₅₁₂, and VVS₁₀₂₄. They exhibit similar tendencies to the module-wise ablation studies of VVS₃₈₄₀ presented in the main script, as shown in Table F, Table G, and Table H. Specifically, within these tables, each module (b)–(d) presents improvements over the baseline (a). In addition, when modules are paired with one another (e)–(g) and when all modules are combined (h), further improvements can be ob-

VVS₅₀₀	<i>Elim.</i>		<i>Gen.</i>		FIVR-5K		
	DDM	TSM	TGM	DSVR	CSVVR	ISVR	
(a)				0.605	0.615	0.580	
(b)	✓			0.626	0.637	0.598	
(c)		✓		0.611	0.620	0.585	
(d)			✓	0.621	0.632	0.599	
(e)	✓	✓		0.624	0.635	0.602	
(f)	✓	✓		0.632	0.641	0.603	
(g)	✓		✓	0.635	0.646	0.619	
(h)	✓	✓	✓	0.636	0.648	0.620	

Table F: **Module-wise Ablations for VVS₅₀₀**. *Elim.* refers to the easy distractor elimination stage, and *Gen.* refers to the suppression weight generation stage. (a) represents a baseline of the same dimension that weights all frames equally without any of the proposed modules, (b)-(g) represents module-wise ablations, and (h) represents VVS₅₀₀.

VVS₅₁₂	<i>Elim.</i>		<i>Gen.</i>		FIVR-5K		
	DDM	TSM	TGM	DSVR	CSVVR	ISVR	
(a)				0.606	0.616	0.580	
(b)	✓			0.626	0.637	0.598	
(c)		✓		0.612	0.621	0.585	
(d)			✓	0.623	0.633	0.600	
(e)	✓	✓		0.625	0.635	0.602	
(f)	✓	✓		0.632	0.643	0.603	
(g)	✓		✓	0.638	0.647	0.619	
(h)	✓	✓	✓	0.643	0.654	0.625	

Table G: **Module-wise Ablations for VVS₅₁₂**. *Elim.* refers to the easy distractor elimination stage, and *Gen.* refers to the suppression weight generation stage. (a) represents a baseline of the same dimension that weights all frames equally without any of the proposed modules, (b)-(g) represents module-wise ablations, and (h) represents VVS₅₁₂.

served. These results suggest that even if the entire framework operates with reduced dimensions, the proposed modules are still effective.

B.9. Additional Qualitative Results

This section describes qualitative results on the FIVR-5K in addition to those presented in the main script, as depicted in Figure F. These results reveal that the proposed approach effectively suppresses irrelevant frames in untrimmed videos containing a wide variety of content, as intended in the original design.

First, when observing the gray areas erased as easy distractors by DDM, it can be seen that they mainly indi-

VVS₁₀₂₄	<i>Elim.</i>		<i>Gen.</i>		FIVR-5K		
	DDM	TSM	TGM	DSVR	CSVVR	ISVR	
(a)				0.642	0.650	0.609	
(b)	✓			0.662	0.672	0.628	
(c)		✓		0.645	0.653	0.616	
(d)			✓	0.654	0.665	0.631	
(e)	✓	✓		0.656	0.666	0.635	
(f)	✓	✓		0.668	0.676	0.636	
(g)	✓		✓	0.672	0.682	0.653	
(h)	✓	✓	✓	0.678	0.688	0.652	

Table H: **Module-wise Ablations for VVS₁₀₂₄**. *Elim.* refers to the easy distractor elimination stage, and *Gen.* refers to the suppression weight generation stage. (a) represents a baseline of the same dimension that weights all frames equally without any of the proposed modules, (b)-(g) represents module-wise ablations, and (h) represents VVS₁₀₂₄.

cate frames with a lack of visual information. Specifically, frames containing simply text or logos are eliminated, such as the first and eighth frames of the video with the topic “Rooftop restaurant fire”. In addition, due to rapid movement during recording, such as in the eighth and ninth frames of the video with the topic “Truck terror”, the complete blur frames are also removed. Furthermore, frames containing limited information, such as the seventh and ninth frames of the video with the topic “Earthquake in city”, are excluded. Because these cases provide insufficient knowledge for recognizing topics, they should be ignored when describing distinct video-level features.

Moreover, when observing the suppression weights generated by TSM and TGM, the scales of the weights fluctuate based on the degree to which each frame is related to the topic. Specifically, high weight values are assigned because they give a meaningful clue even if the region involved in the topic is in picture-in-picture form, such as the third and fourth frames of the video with the topic “Gun rampage in city”. Additionally, even when a specific person is interviewed about the topic, such as in the second and third frames of the video with the topic “Seaplane crash”, it is assigned low weight values because the event pertaining to the topic is not visually displayed and may be seen in other topic videos. Furthermore, frames that are associated with the topic but do not explicitly depict a rescue activity, such as the fifth frame of the video with the topic “Avalanche rescue”, are given a relatively low weight, whereas frames in which the activity occurs are given high weights. From the above instances, it is clear that the suppression weights determine the amount to which a frame is excluded depending on how directly it connects to the event indicated by the topic for each frame.



Figure F: Additional Qualitative Results on FIVR-5K. The orange line refers to the weights from TSM and TGM; the lower the value, the more suppressed the frame. The gray region corresponds to easy distractors eliminated by DDM, and frames that belong to this area are denoted by a red border.

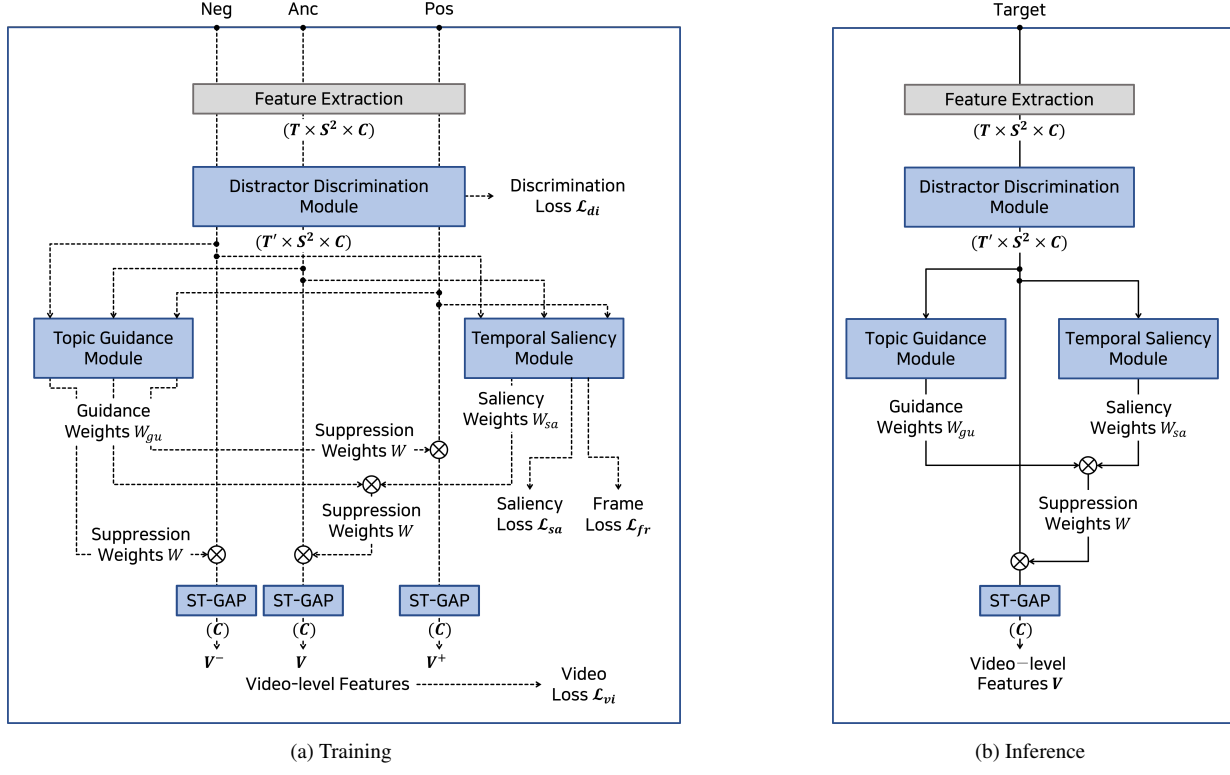


Figure G: **Detailed Pipeline of VVS.** V , V^+ , and V^- refer to the video-level features of anchor, positive, and negative belonging to a triplet, respectively. \otimes refers to the Hadamard product.

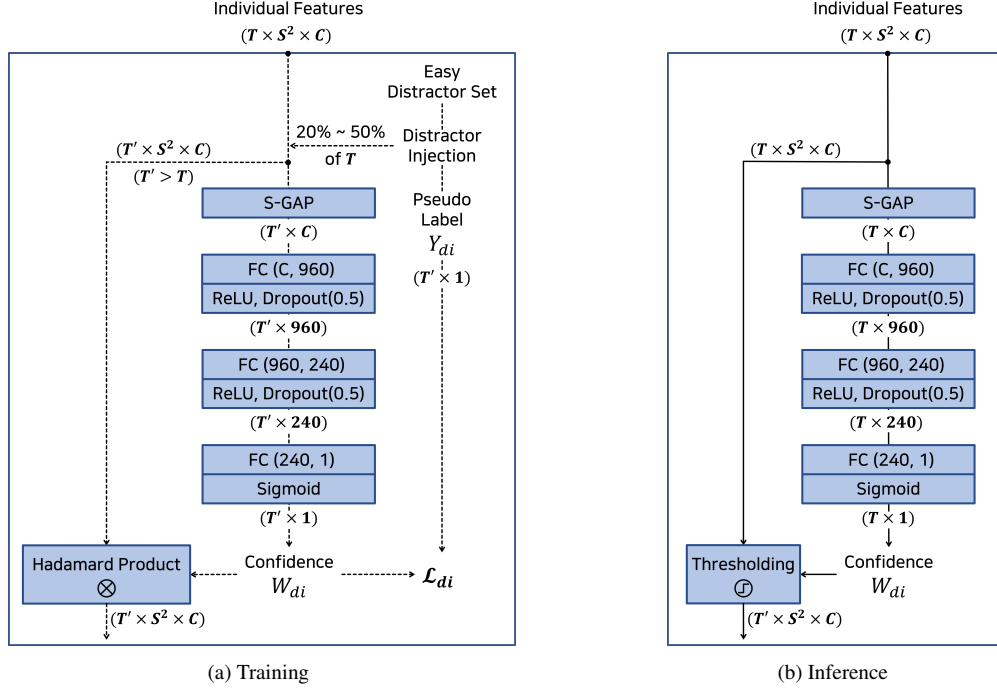


Figure H: **Detailed Pipeline of DDM.** The number in parentheses in FC layer blocks indicates the input and output dimensions. The number in parentheses in dropout layer blocks indicates the probability of an element being zeroed.

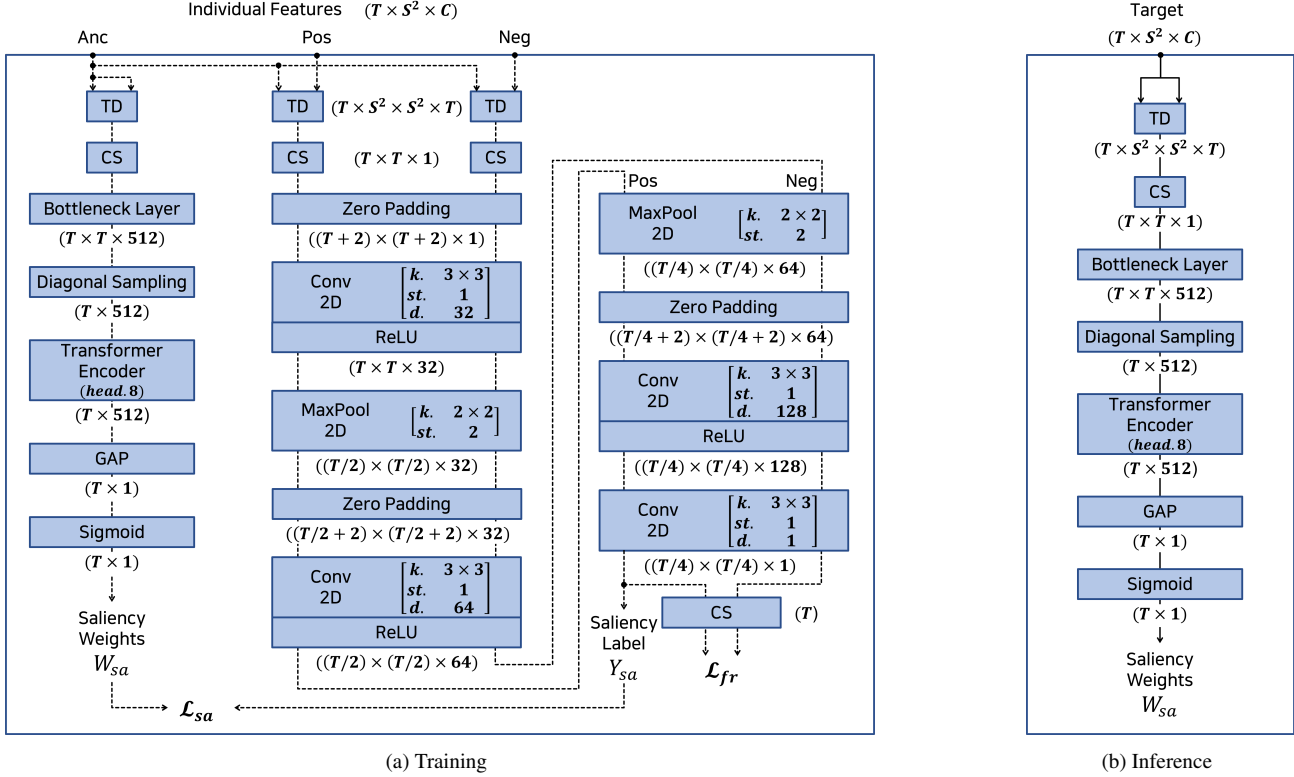


Figure I: **Detailed Pipeline of TSM.** The parentheses in each layer block indicate the parameters for that block. $k.$ denotes kernel size, $st.$ stride, $d.$ dimension, and $head.$ the number of heads in the multi-head attention within the transformer encoder.

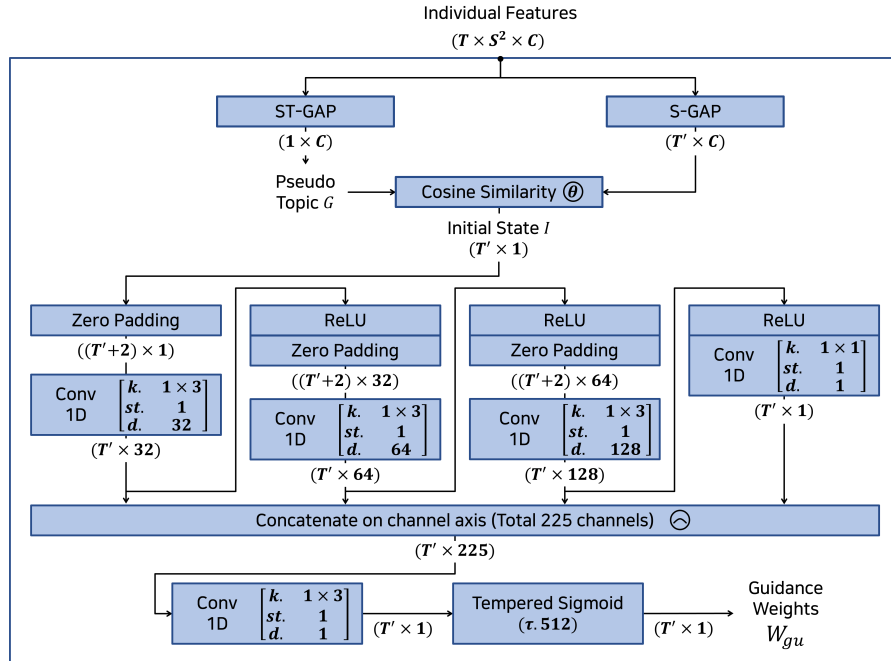


Figure J: **Detailed Pipeline of TGM.** The same pipeline is used for training and inference. The parentheses in each layer block indicate the parameters for that block. $k.$ denotes kernel size, $st.$ stride, $d.$ dimension, and $\tau.$ the temperature of the tempered sigmoid.